Phase-specific manipulation of neural oscillatory activity by transcranial alternating current stimulation

Marina Fiene[a], Bettina C. Schwab[a], Jonas Misselhorn[a], Christoph S. Herrmann[b,c], Till R. Schneider[a], Andreas K. Engel[a]

[a] Department of Neurophysiology and Pathophysiology, University Medical Center Hamburg-Eppendorf, Hamburg, 20246 Germany; [b] Experimental Psychology Lab, Department of Psychology, Cluster of Excellence "Hearing4all", European Medical School, Carl von Ossietzky University Oldenburg, Oldenburg, 26129 Germany; [c] Research Center Neurosensory Science, Carl von Ossietzky University Oldenburg, Oldenburg, 26129 Germany

Corresponding author

Marina Fiene

Department of Neurophysiology and Pathophysiology, University Medical Center Hamburg-Eppendorf

Martinistraße 52, 20246 Hamburg, Germany

Phone: +49 (0)40 7410-54680

Email: m.fiene@uke.de

Keywords

Transcranial alternating current stimulation, Electroencephalogram, Entrainment, Alpha oscillations, Visual flicker

Abstract

Background: Oscillatory phase has been proposed as a key parameter defining the spatiotemporal structure of neural activity. To enhance our understanding of brain rhythms and improve clinical outcomes in pathological conditions, phase-specific modulation of oscillations by transcranial alternating current stimulation (tACS) emerged as a promising approach. However, the effectiveness of tACS in humans is still critically debated.

Objective: Here, we investigated the phase-specificity of tACS effects on visually evoked steady state responses (SSRs) in 24 healthy human participants of either sex.

Methods: To this end, we used an intermittent electrical stimulation protocol and assessed the influence of tACS on SSR amplitude in the interval immediately following tACS.

Results: We observed that the phase shift between flicker and tACS modulates evoked SSR amplitudes. The tACS effect size was dependent on the strength of flicker-evoked oscillatory activity, with larger effects in participants showing weaker locking of neural responses to flicker phase. Neural sources of phase-specific effects were localized in the parieto-occipital cortex within flicker-entrained regions. Importantly, the optimal phase shift between flicker and tACS associated with strongest SSRs was correlated with cortical SSR onset delays over the visual cortex.

Conclusions: Overall, our data provide electrophysiological evidence for phase-specific modulations of oscillatory activity by tACS in humans. As the optimal timing of tACS application was dependent on neural conduction times as measured by SSR onset delays, data suggest that the interaction between tACS effect and SSR was cortical in nature. These findings corroborate the physiological efficacy of tACS and highlight its potential for controlled modulations of brain signals.

Introduction

Oscillations are a prominent feature of activity in neural networks proposed to be of particular importance for neural processing and, by extension, for normal and pathological brain function [1–4]. Modulation of such cortical activity by means of non-invasive brain stimulation represents a promising approach to advance knowledge on the functional role of the temporal patterning of neural activity and to improve clinical outcomes in disorders related to aberrant neural synchrony. Specifically, transcranial alternating current stimulation (tACS) is widely applied with the aim to entrain neural activity, implying a periodic modulation of membrane potentials and a phase alignment of intrinsic oscillations to the tACS phase. This assumption is supported by in vitro slice preparations and recordings in primates showing phase-specific modulations of neuronal spiking patterns by externally applied electric fields [5–8]. However, evidence from invasive recordings in animals may not directly be transferable to tACS effects in the human brain. Despite its broad use in basic and clinical science, the neural mechanism of tACS in humans is still under investigation and its overall efficacy has recently been challenged. Measurements of the electric field strength in human cadaver brains and epilepsy patients with implanted electrodes showed that most of the scalp-applied current is attenuated by skin and skull thereby questioning significant neural entrainment [9–11]. These findings, paralleled by inconsistent behavioral tACS effects [12–14], encouraged a reconsideration of study requirements to investigate the physiological mechanisms of tACS.

The theoretically ideal approach to directly measure tACS-induced effects on neural activity is complicated by strong, hard-to-predict electrical artifacts in concurrent recordings of neural activity [15,16]. To provide evidence for online phase-specific neuronal effects despite these methodological constraints, most studies assessed tACS effects on indirect measures assumed to be mediated by brain rhythms. For instance, tACS applied in the alpha and beta range was shown to lead to cyclic modulations of auditory, somatosensory or visual stimulus perception [17–20]. Further insight has been provided in the motor domain, by showing tACS-phase-

75 dependent changes in cortical excitability [21–23] or peripheral tremor [24–26]. Yet, tACS-
76 effects on the motor cortex were shown to be dominated by cutaneous co-stimulation of
77 peripheral nerves in the skin leading to rhythmic activation of the somatosensory system rather
78 than by transcranial modulation of cortical tissue [27]. Related evidence might thus not
79 necessarily be generalizable to transcranial entrainment effects in cortical regions apart from
80 the motor cortex. Further, prior conclusions only hold true under the assumption that the chosen
81 outcome measures, e.g., behavior or cortical excitability, are reliable proxies for cortical
82 oscillatory activity.

83 Here, we used an innovative approach that combines rhythmic electrical with rhythmic
84 sensory stimulation to target the phase-specificity of tACS effects directly on cortical
85 oscillatory activity. Via electroencephalography (EEG), we measured neural tACS effects on
86 precisely controlled brain rhythms evoked by visual flicker, i.e., visually evoked steady state
87 responses (SSRs), as a function of six phase shifts between tACS and flicker onset. Using an
88 intermittent electrical stimulation protocol, concurrent 10 Hz flicker and multi-electrode tACS
89 targeting the occipital cortex were applied in two sessions under active and sham tACS. Artifact
90 free epochs in the immediate interval following tACS were used for SSR amplitude analysis
91 (Figure 1). We predicted that the phase shift between flicker- and tACS-induced membrane
92 voltage fluctuations should systematically modulate the amplitude of net SSRs.

93

94 **Figure 1.**

95

96 Materials and Methods

97 *Participants*

98 24 healthy volunteers (mean age 25.1 ± 3.3 years; 16 female; 8 male; 22 right-handed) were
99 recruited from the University Medical Center Hamburg-Eppendorf, Germany. The sample size
100 was chosen based on the effect sizes between sham and active tACS in previous studies showing

101 phase-dependent stimulation effects on sensory perception or peripheral tremor [18,24,28]. All
102 participants reported normal or corrected-to-normal vision, no history of psychiatric or
103 neurological disorders and were blind towards the tACS stimulation sequence. The
104 experimental protocol was approved by the ethics committee of the Hamburg Medical
105 Association and was conducted in accordance with the Declaration of Helsinki. All participants
106 gave written informed consent before participation. Participants were monetarily compensated
107 and debriefed immediately after the experiment.
108
109 *Experimental design*
110 All subjects participated in two separate sessions in a randomized, counterbalanced order
111 once under sham and active tACS. Participants were seated in a dimly lit, electrically shielded
112 and sound-attenuated EEG chamber at a distance of approximately 40 cm to a white light
113 emitting diode (LED). Due to a nonlinear relation between forward voltage and luminosity of
114 the used LED, we assessed LED luminosity per duty cycle of the pulse-width modulation by a
115 luminance meter (LS-100, Konica Minolta). The resulting function was multiplied with a pure
116 10 Hz sine to generate a 10 Hz luminance signal. The LED had a maximal light intensity of 100
117 cd/m^2. Prior to the main tACS block, 3 min eyes-open resting state EEG (Pre RS) was recorded
118 while participants fixated the white illuminated LED. Afterwards, EEG during an 8 min SSR
119 block without tACS (Pre SSR) was recorded. Single flicker periods (50 in total) were presented
120 for 5.5 sec followed by short breaks of 3-5 sec. The timing of flicker presentation was identical
121 to the procedure used in the main tACS block. In the tACS block, EEG was recorded
122 continuously during the intermittent tACS protocol. Each trial started with tACS only and was
123 followed by flicker onset after 3-5 sec. The flicker continued until the end of the trial for 5.5
124 sec in total. tACS free intervals of 2.5 sec were used for EEG data analysis. Single tACS periods
125 had a duration of 6-8 sec. Between successive tACS epochs, tACS phase was continuous by
126 adjusting only the amplitude but not the phase of the sine wave spanning the whole testing

127 session. To account for the varying phase delay between neural activity induced by sensory and
128 electrical stimulation, the visual flicker started at six different phase angles (0°, 60°, 120°, 180°,
129 240° and 300°) relative to the tACS cycle. 50 trials were recorded for each of the six phase shift
130 conditions (300 trials in total). The sequence of trials was randomized such that every phase
131 shift condition was followed equally likely by all other conditions. Moreover, to avoid
132 confounding time-on-task effects on alpha amplitude, trials belonging to different conditions
133 were evenly distributed over the course of the testing session by iterate permutation. The tACS
134 block was divided in two blocks interrupted by a 10 min break. After the tACS block, another
135 SSR block without tACS (Post SSR) and resting state EEG (Post RS) were recorded.

136 To ensure that participants fixate the LED and thus to enhance SSR detection, participants
137 were instructed to detect oddball trials in which LED luminance changed after 3-4 sec.
138 Participants responded per button press as soon as they detected a luminance change. 16 oddball
139 trials were included in the tACS block and two oddball trials in the pre and post SSR blocks,
140 respectively. Participants showed a mean detection accuracy of 97.66 ± 9.99 % (mean ± sd)
141 during the tACS blocks and 97.92 ± 12.39 % during the pre and post SSR blocks.

142

143 *Electrophysiological recording*

144 EEG was recorded continuously from 64 Ag/AgCl electrodes (12 mm diameter) mounted
145 in an elastic cap (Easycap). The electrooculogram (EOG) was recorded from two electrodes
146 placed below both eyes with the EEG referenced to the nose tip. Electrodes were prepared with
147 abrasive conducting gel (Abralyt 2000, Easycap) keeping impedance below 20 kΩ. EEG data
148 were recorded using BrainAmp DC amplifiers (Brain Products GmbH) and the corresponding
149 software (Brain Products GmbH, Recorder 1.20). Data were recorded with an online passband
150 of 0.016-250 Hz and digitized with a sampling rate of 1000 Hz.

151

152

153 *tACS and electric field simulation*

154 Multi-electrode tACS was applied via five additional Ag/AgCl electrodes (12 mm diameter)
155 mounted between EEG electrodes. The montage was connected to a battery-driven current
156 source (DC-Stimulator Plus, NeuroConn). After preparation with Signa electrolyte gel (Parker
157 Laboratories Inc.), impedance of each outer electrode to the middle electrode was kept below
158 20 kΩ. Moreover, impedances were kept comparable to achieve an evenly distributed electric
159 field. A sinusoidal alternating current of 2 mA peak-to-peak was applied at 10 Hz using an
160 intermittent stimulation protocol. It has previously been shown that flicker-evoked SSRs show
161 strongest amplitudes in the alpha frequency range [29]. Also, most reliable evidence for
162 aftereffects of tACS on oscillatory power has been demonstrated in the alpha band that was
163 proposed to result from online neural phase-alignment [30,31]. Thus, we chose 10 Hz to test
164 for the general feasibility of phase-specific effects by tACS, although our approach is not
165 limited to this stimulation frequency. During sham and active stimulation, the current was
166 ramped in over 15 sec to 2 mA. After 90 sec of continuous stimulation, tACS periods of 6-8
167 sec without ramp were applied interrupted by short breaks of 2.5 sec for EEG analysis. Total
168 stimulation time during the active session was 40 min. For sham stimulation, the current was
169 ramped in and out over 15 sec each. This procedure ensured that in both stimulation conditions,
170 participants experienced initial itching sensation. All participants confirmed that stimulation
171 was acceptable and did not induce painful skin sensations. The most common side-effect was
172 a tingling feeling on the scalp under the electrode. During the debriefing at the end of the final
173 session, except for two subjects all participants correctly rated the sequence of active and sham
174 stimulation. Further, exploration of the experience of phosphenes during tACS in the beginning
175 of each session revealed that no participant reported phosphene perception. This finding is in
176 line with our simulation of the tACS-induced electric field which greatly diminishes with
177 increasing distance to stimulation electrodes and is expected to be low in the retina [32].

178 Placement of tACS electrodes was chosen to target brain regions activated by visual
179 stimulation. We aimed to achieve largest magnitudes of current density in the primary visual
180 cortex to maximally interfere with early stages of cortical sensory processing. Quantitative field
181 distributions $\vec{E}$ could directly be computed by linear superposition of lead fields $\vec{L}$, weighted by
182 the injected currents α_i at electrodes $i = \{1,2,3,4,5\}$:
183
184 $$\vec{E}(\vec{x}) = \sum_i (\overrightarrow{L_i}\,(\vec{x})\,\alpha_i) \quad (1)$$
185
186 $\vec{L}$ was estimated with the boundary element method using a volume conduction model by
187 Oostenveld et al. [33] at 5 mm spatial resolution.
188

189 **Data analysis**

190 *Data preprocessing*

191 64-channel EEG data were preprocessed and analyzed in Matlab (The MathWorks Inc.)
192 using the analysis toolbox FieldTrip [34]. Circular statistics were calculated with the CircStat
193 toolbox [35]. EEG recordings during the pre and post SSR blocks without tACS were
194 segmented into epochs from -1.5 to 6.5 sec around flicker onset. For the tACS block, EEG was
195 segmented into epochs from 0.1 to 2.5 sec after tACS offset. The first 0.1 sec after stimulation
196 offset were rejected before filtering to avoid leakage of capacitive discharge effects after tACS
197 offset, appearing as a short-lasting voltage drift back to baseline EEG level [30,36].
198 Examination of voltage across 20 ms time segments confirmed no further significant voltage
199 offset change beyond 0.1 sec after the end of stimulation. EEG data were bandpass filtered from
200 1 to 20 Hz using a Hamming-windowed sinc FIR filter. Oddball trials and trials during which
201 participants erroneously responded via button press were excluded. To automatically screen for
202 high noise level electrodes, channels whose standard deviation exceeded 3 times the median
203 standard deviation of all channels per participant were excluded. On average, 4.0 ± 1.9 channels
204 were removed. Data were downsampled to 100 Hz. Afterwards, independent component

analysis (ICA) was computed using the infomax ICA algorithm [37]. Remaining eye-movement, cardiac and noise artifacts were removed based on visual inspection of the components' time course, spectrum and topography. For eye-blink artifact removal, Pearson linear correlation coefficient between EOG and ICA components was calculated and components showing correlation coefficients greater than .25 were rejected. On average, 20.1 ± 3.9 components were excluded. Finally, all trials were visually inspected and trials containing artifacts that had not been detected by previous steps were manually removed. On average, 49.19 ± 1.2 out of 50 trials remained for the pre and post SSR blocks and 296.9 ± 3.5 out of 300 trials remained for the tACS block per participant.

Source reconstruction

At the cortical source level, neural activity was estimated using exact low resolution brain electromagnetic tomography (eLORETA). Before source projection, data were bandpass filtered between 7-13 Hz with a 4th order butterworth filter. The cortical grid was defined using the Automated Anatomical Labeling (AAL) atlas consisting of 38 regions after excluding subcortical and cerebellar structures [38]. Three-dimensional time series were estimated in a linearly spaced grid of 4077 cortical points with 7.5 mm distance in all three spatial directions using the boundary element method volume conduction model by Oostenveld et al. [33]. eLORETA was applied per trial with 5% regularization. To reduce spatial dimensions, the three resulting time series were projected to the direction of maximal power at each grid point.

Spectral analysis and SSR amplitude modulation indices

EEG spectral analysis was performed on sensor and source level. We expected to find phase-specific tACS-induced modulations of SSR amplitude at electrode positions showing a clear response to visual flicker, i.e., where phase alignment to flicker stimulation is prominent. Therefore, we assessed the spatial distribution of phase locking of EEG to visual flicker in the

pre SSR blocks without tACS for the sham and active tACS testing session. A Hilbert transform was computed on the flicker signal and EEG time series during flicker stimulation (1.0 to 5.5 sec after flicker onset) for each trial at each electrode and source level grid point. The first 1 sec after flicker onset was removed to ensure the SSR has fully build up. To assess phase stability, the time-dependent differences in phase signals ($\phi_{flicker}(t) - \phi_{EEG}(t)$) were computed and the extent of entrainment quantified by the phase locking value (PLV) over all trials.

$$PLV = \left|\frac{1}{N_{trials}}\sum_{k=1}^{N_{trials}}\left(\frac{1}{N_{time}}\sum_{t=1}^{N_{time}} e^{i(\phi_{flicker}(t) - \phi_{EEG}(t))}\right)\right| \quad (2)$$

For sensor level analysis, we selected those channels showing prominent phase entrainment with mean PLV > 0.5 over all participants. Pearson correlation coefficient was computed to quantify the relation between PLV and SSR amplitude increase from resting state to pre SSR blocks. SSR amplitude was calculated by Fourier transform of 1 sec time windows with an overlap of 0.5 sec for each 3 min resting state block (pre RS) and for each 4.5 sec trial of the pre SSR blocks. To correct for global alpha amplitude fluctuations over time independent of experimental manipulation, SSR amplitude was defined as a relative amplitude value by subtracting the mean amplitude at neighboring frequencies (9 and 11 Hz) from the absolute amplitude at the stimulation frequency.

For analysis of SSR amplitude modulation during the tACS block, we computed the Fourier transform of each trial separately for the time epochs of 0.1 to 1.1 sec, 0.6 to 1.6 sec and 1.1 to 2.1 sec after tACS offset. To assess modulation of SSR amplitude dependent on the relative phase shift between tACS and flicker onset, bar diagrams were constructed showing the variation in SSR amplitude over phase shift conditions. SSR amplitude was normalized by the sum of amplitude values over all six conditions. Assignment of trials to phase conditions for the sham session was performed using the same trial numbers as under tACS stimulation, thereby ensuring equal time-on-task effects for both sessions. If there was no phase-specific

amplitude modulation by concurrent tACS, bar graphs should be uniformly distributed. In case of phase-specific interactions, the SSR amplitude should be higher in a condition that shows an optimal phase shift for that participant. Assuming that the optimal phase shift between flicker and tACS onset leading to increased SSR amplitudes might vary between participants, any preference in phase shift condition compared to sham can be considered as evidence for phase specific tACS effects. Amplitude modulation was quantified by three modulation measures. First, we calculated the Kullback-Leibler divergence (D_{KL}) which is a common premetric used in statistics to calculate the difference between two distributions. The deviation of the observed amplitude distribution *P* from the uniform distribution *U* is defined as

$$D_{KL}(P,U) = \sum_{i=1}^{N} P(i)\ log\left[\frac{P(i)}{U(i)}\right] \tag{3}$$

where *N* is the number of phase bins [39]. Strict uniformly distributed amplitude values would be reflected in $D_{KL} = 0$ whereas D_{KL} increases the further away *P* gets from *U*. While D_{KL} measures the overall deviation of amplitude values from uniform distribution, we additionally assessed whether the tACS-induced amplitude modulation over phase conditions follows a cyclic pattern, as hypothesized based on the sinusoidal nature of the tACS signal. Therefore, we calculated the phase locking value of amplitude values to phase condition. This cyclic amplitude phase locking (APL) index is defined as

$$APL = \left|\sum_b A_b\ e^{i\theta b}\ \right| \tag{4}$$

where A and θ are the normalized relative amplitude and phase shift for each of the six phase shift conditions b. To further investigate whether the tACS-induced SSR amplitude modulation can be described by a sinusoidal pattern, we fitted one-cycle sine waves to SSR amplitude bar diagram values [18,40]. The following equation was fit to the six normalized SSR amplitude values per participant and stimulation condition,

$$y = b + a * \sin(10Hz * 2\pi * x + c) \quad (5)$$

where x corresponds to the flicker-tACS phase shifts during one cycle (x = {0, 1/6T, 2/6T,… 5/6∗T} with period T = 0.1 sec). The parameters a, b and c were estimated by the fitting procedure where b is the intercept, a the amplitude and c the phase shift. Parameters a and b were bound between -1 and 1 and c between 0 and 2π. Start values were drawn randomly from within the range of restrictions for each parameter. Model fits were computed using the Matlab fittype function allowing for 1000 iterations to find the best model. We examined the absolute sine fit amplitude values as index for the strength of SSR amplitude modulation. The significance of the sine fit was assessed by dependent samples t-tests comparing the proportion of explained variance R^2 as goodness-of-fit index between sham and active tACS session.

Statistical analysis

For each of the three modulation indices, we calculated dependent samples t-tests for the epochs of 0.1 to 1.1 sec, 0.6 to 1.6 sec and 1.1 to 2.1 sec after tACS offset between sham and active tACS on sensor level. Effect sizes were determined by calculating Cohen's d_z for paired t-test comparisons. To account for comparisons in multiple time windows, we applied Bonferroni correction to the significance level and report test statistics if the corresponding p-value fell below the corrected alpha of α_{bonf} = .0167 (= .05/3).

For further investigation of tACS effects, we analyzed the APL parameter resulting from the epoch immediately following tACS offset in source space. APL is the more specific, phase-dependent modulation index relative to D_{KL} and a more robust measure not requiring any presuppositions on parameter ranges as compared to sine fit. For source localization of APL effects, dependent samples t-tests were computed for each grid point using cluster-based permutation tests to correct for multiple comparisons. Clusters were obtained by summing up t-values which were adjacent in space and below an alpha level of 5 % (two-sided). A

312 permutation distribution was generated by randomly shuffling APL values between active and
313 sham condition within participants in each of 1000 iterations. The observed cluster was
314 considered statistically significant when the sum of t-values exceeded 95 % of the permutation
315 distribution. To further examine whether the strength of tACS effects quantified by APL is
316 dependent on the underlying strength of flicker-evoked oscillatory activity, we assessed
317 Pearson correlation coefficients between APL and EEG-flicker PLV for sham and active tACS
318 blocks. Moreover, we assessed the dependency of the increase in APL from sham to tACS on
319 the change in mean SSR amplitude, the standard deviation of SSR amplitudes or EEG-flicker
320 PLVs over all trials per participant by computing Pearson correlation coefficients.

321 Finally, to disentangle retinal from cortical stimulation effects, we examined the
322 dependency of optimal flicker-tACS phase shifts on the cortical flicker-SSR phase delays by
323 computing circular-circular correlations per channel using cluster-based permutation tests [35].
324 The flicker-SSR phase delay was computed as the mean time-dependent difference in phase
325 signals ($\phi_{flicker}(t) - \phi_{EEG}(t)$) based on the Hilbert transform of the EEG and flicker signal
326 over all trials of the tACS block. Cluster-level test statistics were calculated by taking the
327 maximum average of correlation coefficients across neighboring electrodes showing
328 significance of circular correlations ($p < .05$). The permutation distribution was generated by
329 between-subject randomization of flicker-tACS and SSR onset phase delay data over 1000
330 iterations.

331

332 **Results**

333 *Flicker-evoked phase alignment in the parieto-occipital cortex*

334 To analyze evoked flicker entrainment, we assessed the degree and spatial distribution of
335 PLVs between EEG and 10 Hz flicker stimulation. Estimated time series on source level
336 displayed a prominent peak of parieto-occipital EEG-flicker PLV (Figure 2B). Strong phase
337 locking was located in the superior and middle occipital gyrus as well as in bilateral precuneus

338 and cuneus. For sensor level analysis, four parieto-occipital channels showing a population
339 mean PLV > 0.5 (corresponding to electrodes O1, O2, POz, Pz) were selected for further
340 analysis of SSR amplitude modulation by tACS. Mean PLV for the selected channels during
341 both pre SSR blocks over all participants was 0.56 ± 0.16 (mean ± sd). As illustrated in the
342 lower part of Figure 2B, data show varying phase delays between flicker onset and cortical SSR
343 across participants related to differences in neural conduction delays along the visual pathway.
344 Further, amplitude spectra revealed an amplitude increase at the flicker stimulation frequency
345 compared to resting state (Figure 2C). Between-subject correlation showed that the strength of
346 EEG-flicker PLV was positively correlated with the increase in SSR amplitude from resting
347 state to pre SSR blocks (r = .43, p = .037) (Figure 2D).
348
349 **Figure 2.**
350
351 *Phase-dependent SSR amplitude modulation by tACS*
352 To test the hypothesis that simultaneous tACS and flicker stimulation lead to phase-specific
353 interactions between evoked neural activity and electric field, we assessed the degree of tACS-
354 phase-dependence of SSR amplitude values via three modulation measures: (1) the deviation
355 of amplitude values from a uniform distribution (D_{KL}), (2) the locking of amplitude values to
356 phase conditions (APL) and (3) one-cycle sine fits to SSR amplitude values. Figure 3A shows
357 normalized SSR amplitude bar diagrams over the six phase shift conditions for one exemplary
358 participant. During sham, data are almost uniformly distributed across phase bins, showing
359 small fluctuations in SSR amplitude with no preference for a particular phase shift condition.
360 On the contrary, the bar diagram for active stimulation shows phase-dependent modulations of
361 SSR amplitudes indicating an interaction between tACS-induced electric field and flicker-
362 evoked oscillatory activity. On sensor level, analysis of the deviation of amplitude values from
363 uniform distribution revealed a significantly greater D_{KL} under tACS compared to sham within

364 the first 1 sec epoch (0.1 to 1.1 sec) after tACS offset ($t(23) = 3.21$, $p = .004 < \alpha_{bonf}$, $d_z = 0.66$)
365 (Figure 3B). Phase locking of amplitude values to phase condition measured by APL was
366 significantly larger after tACS ($t(23) = 3.12$, $p = .005 < \alpha_{bonf}$, $d_z = 0.64$). In accordance, also the
367 one-cycle sine wave fit to SSR amplitudes showed a significantly greater amplitude of the sine
368 fit under tACS ($t(23) = 3.52$, $p = .002 < \alpha_{bonf}$, $d_z = 0.72$) (Figure 3B). The proportion of
369 explained variance R^2 by sine fit was greater for SSR amplitude modulation under tACS
370 compared to sham ($t(23) = 2.65$, $p = .014$, $d_z = 0.54$). In successive time windows, the
371 modulatory tACS effect decayed for all three modulation parameters ([0.6, 1.6] sec: D_{KL}, $t(23)$
372 $= 0.46$, $p = .650$, $d_z = 0.09$; APL, $t(23) = 2.29$, $p = .032$, $d_z = 0.47$; Sine fit, $t(23) = 2.23$, $p =$
373 $.036$, $d_z = 0.45$; [1.1, 2.1] sec: D_{KL}, $t(23) = -0.30$, $p = .769$, $d_z = -0.06$; APL, $t(23) = -0.25$, $p =$
374 $.806$, $d_z = -0.05$; Sine fit, $t(23) = 0.52$, $p = .610$, $d_z = 0.11$; Figure 3E). Importantly, the phase-
375 dependent effects of tACS on SSR amplitude were not caused by overall 10 Hz alpha amplitude
376 differences between conditions (Figure 3C). A repeated-measures t-test revealed no significant
377 difference in mean SSR amplitude ($t(23) = -1.02$, $p = .317$, $d_z = 0.21$) over all trials per
378 participant between tACS and sham condition during the first 1 sec interval after tACS offset
379 (Figure 3D). Also, the standard deviation of SSR amplitude values over all trials per participant
380 did not differ between sham and active stimulation condition ($t(23) = -.31$, $p = .759$, $d_z = 0.06$).
381 This implies a strengthening or dampening of SSR amplitudes dependent on the phase shift
382 between flicker and tACS stimulation.
383
384 **Figure 3.**
385
386 *Spatial localization and dependency of tACS effects on individual physiology*
387 The spatial specificity of tACS effects was analyzed in source space for the APL modulation
388 parameter. Compared to D_{KL}, APL is a more specific index assuming systematic amplitude
389 modulations by tACS. Moreover, its computation is more stable compared to sine fit as no

390 assumptions about parameter ranges are required. Cluster analysis in source space showed
391 significantly increased APL values during active tACS relative to sham in a cluster over the
392 parieto-occipital cortex (cluster test: $p = .006$) (Figure 4A). Significant differences were located
393 primarily in the bilateral precuneus, superior parietal gyrus and midcingulate area as well as the
394 cuneus and calcarine sulcus. These are part of flicker-entrained brain areas, located in tACS-
395 targeted cortical regions and connected higher visual areas. Interestingly, tACS effects on SSR
396 amplitude were not seen in the middle and superior occipital gyrus where neural phase
397 alignment to the visual flicker peaked, but rather in neighboring occipital and parietal regions
398 (insert in Figure 4B).

399 In accordance with this finding, we further observed a highly significant between-subject
400 correlation of SSR amplitude modulation quantified by APL with the underlying strength of
401 EEG-flicker PLV during the active tACS block on sensor level ($r = -.65$, $p < .001$). Participant
402 with weaker PLV of SSR to flicker phase showed greater APL under tACS (Figure 4B). This
403 relation was non-significant during the sham session ($r = -.38$, $p = .067$). As the difference in
404 PLV between sham and tACS session showed no significant correlation with the difference in
405 corresponding APL values ($r = -.29$, $p = .166$), data suggest that the strong negative relation
406 between underlying PLV and SSR modulation is not generally valid but specific for tACS-
407 induced neuromodulation. Our results thus emphasize the impact of the individual physiology,
408 influenced by the neuronal response strength to visual flicker, for the detection of neural tACS
409 effects.

410 Importantly, the increase in APL from sham to tACS could not be explained by a concurrent
411 increase in mean SSR amplitude ($r = -.22$, $p = .309$) or standard deviation of SSR amplitude
412 values ($r = -.13$, $p = .556$) over all trials of the tACS blocks per participant, thereby supporting
413 the causal influence of the experimental manipulation of tACS-flicker phase shift (Figure 4C).
414

415 **Figure 4.**

416 *Cortical level of interaction between SSRs and tACS effects*

417 To examine the involvement of retinal co-stimulation on SSR amplitude modulation, we
418 analyzed the dependency of optimal flicker-tACS phase shifts associated with strongest SSRs
419 on individual flicker-SSR phase delays resulting from neural conduction times from the retina
420 to visual cortex. Assuming an interaction between flicker and electric field at the retinal level
421 before conduction delays of the visual system take effect, the SSR phase delay should have no
422 predictive value for the optimal timing of tACS application. Notably, only during the tACS
423 session, permutation tests revealed a significant cluster of occipital electrodes (O1, O2, O9,
424 O10; cluster test: $p = .009$) showing a circular correlation between SSR phase delay and optimal
425 flicker-tACS phase shift across participants. The mean correlation coefficient across cluster
426 electrodes was $r = -.54$. Corresponding permutation tests during sham showed no significant
427 electrode cluster.

428

429 **Figure 5.**

430

431 **Discussion**

432 Here, we used an innovative approach to study the phase-specificity of electrophysiological
433 tACS effects in humans by systematically pairing rhythmic electrical with rhythmic visual
434 stimulation. Specifically, we evaluated the amplitude of flicker-evoked SSRs in the interval
435 immediately following tACS delivered at six different phase shifts relative to flicker onset. We
436 demonstrate that SSR amplitudes are modulated in a tACS phase-dependent manner and that
437 tACS effect size is inversely related to the strength of the underlying flicker response.
438 Furthermore, we found that the individual phase delay between flicker onset and cortical SSR
439 is predictive of the optimal timing of tACS application.

440 Previous investigations into the tACS mechanism of action typically aimed to modulate
441 ongoing or task-related brain oscillations which show high variability in frequency and phase

consistency. Here, we used SSRs that allow the precise setting of the oscillatory phase in the visual cortex. While the neural mechanism underlying SSR generation is still debated, increasing evidence supports the involvement of entrained endogenous oscillations in the processing of rhythmic visual input [41–43]. Yet, irrespective of their exact physiological origin, SSRs can be treated as stimulus-driven brain rhythms with predictable time course, which enables a highly specific targeting by tACS. Notably, compared to ongoing activity, the phase of the SSR is not expected to be shifted by tACS as EEG recordings will always show dominant phase locking to the driving flicker. Rather, if voltage modulations by electrical and sensory stimulation interact in a phase-specific manner, SSRs should reflect this interaction in net amplitude modulations. Our data confirmed that SSR amplitudes measured immediately after tACS offset are dependent on the relative phase shift between flicker and tACS which provides first conclusive evidence for the phase-specificity of tACS effects in human EEG recordings. Importantly, as data show no overall amplitude increase of SSRs by tACS (Figure 3D), results imply a phase-dependent enhancement and suppression of flicker responses due to the sinusoidal nature of the tACS signal. This is in accordance with recent invasive recordings in animals, showing that tACS is capable of modulating the timing of neural spike discharges [7,8].

The phase-dependent modulatory effect on SSRs was robust under three modulation measures but already decayed after the first 1 sec time epoch. While lasting power enhancement after prolonged alpha tACS has been repeatedly shown and ascribed to synaptic plasticity mechanisms [30,31,44], evidence for outlasting effects on phase synchronization is still sparse. Yet, neural oscillatory activity entrained during rhythmic electric, magnetic or visual stimulation were shown to remain stable for a few cycles after stimulation offset [45–47]. These short-lived reverberations of oscillatory activity, phase-locked to the external force, have been termed entrainment echoes [36,46]. Notably, Vossen et al. [30] could not find evidence for entrainment echoes after short tACS epochs of 3 or 8 sec length. However, while tACS phase

468 effects might not be detectable via PLV in ongoing brain activity, flicker-induced brain rhythms
469 may increase the signal-to-noise ratio and thereby enhance the detectability of short-lived tACS
470 aftereffects. These results are compatible with the assumption of online tACS-induced
471 entrainment of neural activity, which yet cannot be tested directly due to artifact-contaminated
472 EEG recordings. We speculate that the observed effects generalize to tACS and SSRs in other
473 frequency bands of the human EEG, which should be systematically tested in future studies.
474 Interestingly, the efficacy of tACS was inversely related to the strength of the underlying
475 flicker response. More precisely, tACS-induced SSR amplitude modulation was stronger in
476 participants showing weaker phase locking between flicker and evoked oscillatory activity.
477 Furthermore, tACS effects were especially prominent in brain areas that were not maximally
478 driven by the driving flicker. While maximal phase locking to the visual stimulus occurred in
479 the middle and superior occipital gyrus, maximal SSR amplitude effects of tACS were seen in
480 early visual cortex and superior parietal cortex. As tACS effects were also observed in
481 downstream visual cortical areas, these results suggest that stimulation effects might not only
482 act locally in regions targeted by the electric field but also affect connected areas via
483 polysynaptic interactions [48–50]. Moreover, these findings emphasize a dependency of tACS
484 effects on the individual physiology. It has repeatedly been demonstrated that tACS effect sizes
485 are related to the baseline level of oscillatory activity, with effects only being measurable when
486 power at the stimulated frequency was low [51–53]. Similarly, our data indicate that in
487 participants and anatomical regions exhibiting strong EEG-flicker phase locking, the
488 dominance of synchronous neural activity may have led to ceiling effects in alpha amplitude
489 with no room for further enhancement. Also, the ratio between the strength of the external tACS
490 stimulation relative to the strength of the neural oscillation was suggested as a critical factor for
491 successful entrainment [53], that may explain differential tACS effect sizes for varying flicker-
492 evoked oscillation strengths.

493 Important to consider in the interpretation of tACS effects is the possible involvement of
494 sensory co-stimulation effects, that may indirectly lead to neural entrainment. First, electric
495 stimulation of peripheral nerves in the skin can induce rhythmic activation of the somatosensory
496 cortex that was shown to at least partly explain tACS effects on motor cortex [27]. Yet, recent
497 studies demonstrated that tACS affects neural activity even if somatosensory input is controlled
498 for [7,54]. In our study, the dependency of tACS effects on the SSR phase delay over the
499 primary visual cortex, i.e., the target region of the electrical stimulation, point to transcranial
500 stimulation effects on SSR at early stages of visual cortical processing with concurrent spread
501 of activity to higher visual areas. However, to rule out entirely that SSRs were influenced by
502 somatosensory co-stimulation, a control electrode montage would be necessary that elicits
503 equivalent tactile sensation without stimulating the cortex. This is challenging as cutaneous
504 stimulation effects depend not only on current strength but also on the distribution and
505 sensitivity of skin receptors in the stimulated area [55]. Therefore, the development of valid
506 control montages is one of the key goals in future tACS research. Second, it has been noted that
507 tACS can cause activation of the retinae due to shunting of scalp-applied currents across the
508 skin. Although no participant reported phosphene sensation with the used focal ring montage,
509 sub-threshold activation of the retinae could in principle have an impact on visual processing,
510 which was previously dealt with by using control electrode montages [55]. Here, our
511 experimental approach allowed to directly disentangle cortical from retinal stimulation effects.
512 It is well known that flicker stimulation will inevitably lead to variable delays in the recordable
513 SSR that likely result from interindividual differences of the conduction times along the visual
514 pathway. Accordingly, a cortical interaction between tACS effects and SSRs should be
515 associated with varying optimal phase shifts between tACS and flicker across participants. This
516 was exemplified in a study by Ruhnau et al. [56], showing that simultaneously started tACS
517 and flicker did not lead to tACS-induced power increases of the fundamental SSR component
518 in the overall sample. In our study, we could show that the optimal flicker-tACS phase shift

associated with strongest SSRs was correlated with the individual flicker-SSR phase delay over the primary visual cortex. This finding suggests that it is possible to predict the optimal timing of tACS application based on subject-specific conduction delays of the visual system. Importantly, this dependency cannot be explained by an interference between flicker and electric field at the retinal level, which should be independent of postretinal neural conduction times and, therefore, result in comparable optimal flicker-tACS phase shifts across participants. Thus, our finding strongly suggests that the interaction between tACS effect and SSR was cortical rather than retinal in nature.

In conclusion, we provide the first conclusive electrophysiological evidence for the efficacy of tACS to modulate cortical oscillatory activity in a phase-dependent manner in humans. Importantly, we found that the optimal phase shift between electrical and visual stimulation varied between participants and depended on baseline conduction delays of the visual system. This result cannot be explained by peripheral electric co-stimulation of the retina and thus strongly supports a cortical origin of tACS effects. Furthermore, our data corroborate the notion that tACS effect size is limited by the strength of the targeted oscillatory activity level. Taken together, our findings show that individual functional properties and the current oscillatory brain state need to be considered to achieve specific, custom-fit neuromodulation. In the context of the ongoing debate on the overall capability of tACS to entrain oscillatory activity in humans, our results make a strong case for its periodic impact on neuronal excitability that would allow for frequency- and phase-specific modulations of brain signals.

Conflict of interest

The authors declare no competing financial interests.

Acknowledgements

This work was supported by the Deutsche Forschungsgemeinschaft (SFB 936/A3 awarded to A.K.E. and T.R.S.; SPP 1665/EN 533/13-1 and SFB TRR 169/B1 awarded to A.K.E.; SPP 1665/SCHN 1511/1-2 awarded to T.R.S.). We thank Jonathan Daume, Alexander Maye, Jan-Ole Radecke and Darius Zokai for helpful discussions on the data, Malte Sengelmann and Guido Nolte for methodological support, and Karin Deazle and Darius Zokai for assistance in data recording.

References

[1] Fries P. A mechanism for cognitive dynamics: Neuronal communication through neuronal coherence. Trends Cogn Sci 2005;9:474–80. https://doi.org/10.1016/j.tics.2005.08.011.

[2] Schnitzler A, Gross J. Normal and pathological oscillatory communication in the brain. Nat Rev Neurosci 2005;6:285–96. https://doi.org/10.1038/nrn1650.

[3] Ronconi L, Melcher D. The role of oscillatory phase in determining the temporal organization of perception: Evidence from sensory entrainment. J Neurosci 2017;37:10636–44. https://doi.org/10.1523/JNEUROSCI.1704-17.2017.

[4] Engel AK, Fries P, Singer W. Dynamic predictions: Oscillations and synchrony in top–down processing. Nat Rev Neurosci 2001;2:704–16. https://doi.org/10.1038/35094565.

[5] Ali MM, Sellers KK, Fröhlich F. Transcranial alternating current stimulation modulates large-scale cortical network activity by network resonance. J Neurosci 2013;33:11262–75. https://doi.org/10.1523/JNEUROSCI.5867-12.2013.

[6] Reato D, Rahman A, Bikson M, Parra LC. Effects of weak transcranial alternating current stimulation on brain activity—a review of known mechanisms from animal studies. Front Hum Neurosci 2013;7:687. https://doi.org/10.3389/fnhum.2013.00687.

[7] Krause MR, Vieira PG, Csorba BA, Pilly PK, Pack CC. Transcranial alternating current stimulation entrains single-neuron activity in the primate brain. Proc Natl Acad Sci 2019:201815958. https://doi.org/10.1073/pnas.1815958116.

[8] Johnson L, Alekseichuk I, Krieg J, Doyle A, Yu Y, Vitek J, et al. Dose-dependent effects of transcranial alternating current stimulation on spike timing in awake nonhuman primates. BioRxiv:696344 2019. https://doi.org/10.1101/696344.

[9] Vöröslakos M, Takeuchi Y, Brinyiczki K, Zombori T, Oliva A, Fernández-Ruiz A, et al. Direct effects of transcranial electric stimulation on brain circuits in rats and humans. Nat Commun 2018;9:483. https://doi.org/10.1038/s41467-018-02928-3.

581 [10] Huang Y, Liu AA, Lafon B, Friedman D, Dayan M, Wang X, et al. Measurements and
582 models of electric fields in the in vivo human brain during transcranial electric
583 stimulation. Elife 2017;6:1–26. https://doi.org/10.7554/eLife.18834.
584 [11] Underwood E. Cadaver study challenges brain stimulation methods. Science
585 2016;352:397–397. https://doi.org/10.1126/science.352.6284.397.
586 [12] Brignani D, Ruzzoli M, Mauri P, Miniussi C. Is transcranial alternating current
587 stimulation effective in modulating brain oscillations? PLoS One 2013;8:e56589.
588 https://doi.org/10.1371/journal.pone.0056589.
589 [13] Fekete T, Nikolaev AR, De Knijf F, Zharikova A, van Leeuwen C. Multi-electrode alpha
590 tACS during varying background tasks fails to modulate subsequent alpha power. Front
591 Neurosci 2018;12:428. https://doi.org/10.3389/fnins.2018.00428.
592 [14] Vossen A. Modulation of neural oscillations and associated behaviour by transcranial
593 alternating current stimulation (tACS). PhD thesis. 2017.
594 [15] Noury N, Hipp JF, Siegel M. Physiological processes non-linearly affect
595 electrophysiological recordings during transcranial electric stimulation. Neuroimage
596 2016;140:99–109. https://doi.org/10.1016/j.neuroimage.2016.03.065.
597 [16] Noury N, Siegel M. Phase properties of transcranial electrical stimulation artifacts in
598 electrophysiological recordings. Neuroimage 2017;158:406–16.
599 https://doi.org/10.1016/j.neuroimage.2017.07.010.
600 [17] Gundlach C, Müller MM, Nierhaus T, Villringer A, Sehm B. Phasic modulation of
601 human somatosensory perception by transcranially applied oscillating currents. Brain
602 Stimul 2016;9:712–9. https://doi.org/10.1016/j.brs.2016.04.014.
603 [18] Neuling T, Rach S, Wagner S, Wolters CH, Herrmann CS. Good vibrations: Oscillatory
604 phase shapes perception. Neuroimage 2012;63:771–8.
605 https://doi.org/10.1016/j.neuroimage.2012.07.024.
606 [19] Helfrich RF, Schneider TR, Rach S, Trautmann-Lengsfeld SA, Engel AK, Herrmann

607 CS. Entrainment of brain oscillations by transcranial alternating current stimulation. Curr
608 Biol 2014;24:333–9. https://doi.org/10.1016/j.cub.2013.12.041.
609 [20] Riecke L, Formisano E, Herrmann CS, Sack AT. 4-Hz transcranial alternating current
610 stimulation phase modulates hearing. Brain Stimul 2015;8:777–83.
611 https://doi.org/10.1016/j.brs.2015.04.004.
612 [21] Nakazono H, Ogata K, Kuroda T, Tobimatsu S. Phase and frequency-dependent effects
613 of transcranial alternating current stimulation on motor cortical excitability. PLoS One
614 2016;11:e0162521. https://doi.org/10.1371/journal.pone.0162521.
615 [22] Guerra A, Pogosyan A, Nowak M, Tan H, Ferreri F, Di Lazzaro V, et al. Phase
616 dependency of the human primary motor cortex and cholinergic inhibition cancelation
617 during beta tACS. Cereb Cortex 2016;26:3977–90.
618 https://doi.org/10.1093/cercor/bhw245.
619 [23] Schilberg L, Engelen T, ten Oever S, Schuhmann T, de Gelder B, de Graaf TA, et al.
620 Phase of beta-frequency tACS over primary motor cortex modulates corticospinal
621 excitability. Cortex 2018;103:142–52. https://doi.org/10.1016/j.cortex.2018.03.001.
622 [24] Khatoun A, Breukers J, Op de Beeck S, Nica IG, Aerts J-M, Seynaeve L, et al. Using
623 high-amplitude and focused transcranial alternating current stimulation to entrain
624 physiological tremor. Sci Rep 2018;8:8221. https://doi.org/10.1038/s41598-018-26013-
625 3.
626 [25] Mehta AR, Brittain J-S, Brown P. The selective influence of rhythmic cortical versus
627 cerebellar transcranial stimulation on human physiological tremor. J Neurosci
628 2014;34:7501–8. https://doi.org/10.1523/JNEUROSCI.0510-14.2014.
629 [26] Brittain J-S, Probert-Smith P, Aziz TZ, Brown P. Tremor suppression by rhythmic
630 transcranial current stimulation. Curr Biol 2013;23:436–40.
631 https://doi.org/10.1016/j.cub.2013.01.068.
632 [27] Asamoah B, Khatoun A, Mc Laughlin M. tACS motor system effects can be caused by

633 transcutaneous stimulation of peripheral nerves. Nat Commun 2019;10:266.
634 https://doi.org/10.1038/s41467-018-08183-w.
635 [28] Riecke L, Sack AT, Schroeder CE. Endogenous delta/theta sound-brain phase
636 entrainment accelerates the buildup of auditory streaming. Curr Biol 2015;25:3196–201.
637 https://doi.org/10.1016/j.cub.2015.10.045.
638 [29] Herrmann CS. Human EEG responses to 1-100 Hz flicker: Resonance phenomena in
639 visual cortex and their potential correlation to cognitive phenomena. Exp Brain Res
640 2001;137:346–53. https://doi.org/10.1007/s002210100682.
641 [30] Vossen A, Gross J, Thut G. Alpha power increase after transcranial alternating current
642 stimulation at alpha frequency (α-tACS) reflects plastic changes rather than entrainment.
643 Brain Stimul 2015;8:499–508. https://doi.org/10.1016/j.brs.2014.12.004.
644 [31] Zaehle T, Rach S, Herrmann CS. Transcranial alternating current stimulation enhances
645 individual alpha activity in human EEG. PLoS One 2010;5:e13766.
646 https://doi.org/10.1371/journal.pone.0013766.
647 [32] Laakso I, Hirata A. Computational analysis shows why transcranial alternating current
648 stimulation induces retinal phosphenes. J Neural Eng 2013;10:046009.
649 https://doi.org/10.1088/1741-2560/10/4/046009.
650 [33] Oostenveld R, Stegeman DF, Praamstra P, van Oosterom A. Brain symmetry and
651 topographic analysis of lateralized event-related potentials. Clin Neurophysiol
652 2003;114:1194–202. https://doi.org/10.1016/S1388-2457(03)00059-2.
653 [34] Oostenveld R, Fries P, Maris E, Schoffelen J-M. FieldTrip: Open source software for
654 advanced analysis of MEG, EEG, and invasive electrophysiological data. Comput Intell
655 Neurosci 2011;2011:1–9. https://doi.org/10.1155/2011/156869.
656 [35] Berens P. CircStat: A MATLAB toolbox for circular statistics. J Stat Softw 2009;31:1–
657 21.
658 [36] Stonkus R, Braun V, Kerlin JR, Volberg G, Hanslmayr S. Probing the causal role of

659 prestimulus interregional synchrony for perceptual integration via tACS. Sci Rep
660 2016;6:32065.
661 [37] Bell AJ, Sejnowski TJ. Blind separation and blind deconvolution: An information-
662 theoretic approach 2002;5:3415–8. https://doi.org/10.1109/ICASSP.1995.479719.
663 [38] Hahm J, Lee H, Park H, Kang E, Kim YK, Chung CK, et al. Gating of memory encoding
664 of time-delayed cross-frequency MEG networks revealed by graph filtration based on
665 persistent homology. Sci Rep 2017;7:41592. https://doi.org/10.1038/srep41592.
666 [39] Tort ABL, Komorowski R, Eichenbaum H, Kopell N. Measuring phase-amplitude
667 coupling between neuronal oscillations of different frequencies. J Neurophysiol
668 2010;104:1195–210. https://doi.org/10.1152/jn.00106.2010.
669 [40] Wilsch A, Neuling T, Obleser J, Herrmann CS. Transcranial alternating current
670 stimulation with speech envelopes modulates speech comprehension. Neuroimage
671 2018;172:766–74. https://doi.org/10.1016/j.neuroimage.2018.01.038.
672 [41] Keitel C, Keitel A, Benwell CSY, Daube C, Thut G, Gross J. Stimulus-driven brain
673 rhythms within the alpha band: The attentional-modulation conundrum. J Neurosci
674 2019;39:3119–29. https://doi.org/10.1523/JNEUROSCI.1633-18.2019.
675 [42] Notbohm A, Kurths J, Herrmann CS. Modification of brain oscillations via rhythmic
676 light stimulation provides evidence for entrainment but not for superposition of event-
677 related responses. Front Hum Neurosci 2016;10:10.
678 https://doi.org/10.3389/fnhum.2016.00010.
679 [43] Zoefel B, ten Oever S, Sack AT. The involvement of endogenous neural oscillations in
680 the processing of rhythmic input: More than a regular repetition of evoked neural
681 responses. Front Neurosci 2018;12:1–13. https://doi.org/10.3389/fnins.2018.00095.
682 [44] Wischnewski M, Engelhardt M, Salehinejad MA, Schutter DJLG, Kuo MF, Nitsche MA.
683 NMDA receptor-mediated motor cortex plasticity after 20 Hz transcranial alternating
684 current stimulation. Cereb Cortex 2019;29:2924–31.

685 https://doi.org/10.1093/cercor/bhy160.
686 [45] Marshall L, Helgadóttir H, Mölle M, Born J. Boosting slow oscillations during sleep
687 potentiates memory. Nature 2006;444:610–3. https://doi.org/10.1038/nature05278.
688 [46] Hanslmayr S, Matuschek J, Fellner M-C. Entrainment of prefrontal beta oscillations
689 induces an endogenous echo and impairs memory formation. Curr Biol 2014;24:904–9.
690 https://doi.org/10.1016/j.cub.2014.03.007.
691 [47] Halbleib A, Gratkowski M, Schwab K, Ligges C, Witte H, Haueisen J. Topographic
692 analysis of engagement and disengagement of neural oscillators in photic driving. J Clin
693 Neurophysiol 2012;29:33–41. https://doi.org/10.1097/WNP.0b013e318246ad6e.
694 [48] Ozen S, Sirota A, Belluscio MA, Anastassiou CA, Stark E, Koch C, et al. Transcranial
695 electric stimulation entrains cortical neuronal populations in rats. J Neurosci
696 2010;30:11476–85. https://doi.org/10.1523/JNEUROSCI.5252-09.2010.
697 [49] Cabral-Calderin Y, Anne Weinrich C, Schmidt-Samoa C, Poland E, Dechent P, Bähr M,
698 et al. Transcranial alternating current stimulation affects the BOLD signal in a frequency
699 and task-dependent manner. Hum Brain Mapp 2016;37:94–121.
700 https://doi.org/10.1002/hbm.23016.
701 [50] Chai Y, Sheng J, Bandettini PA, Gao J-H. Frequency-dependent tACS modulation of
702 BOLD signal during rhythmic visual stimulation. Hum Brain Mapp 2018;39:2111–20.
703 https://doi.org/10.1002/hbm.23990.
704 [51] Ruhnau P, Neuling T, Fuscá M, Herrmann CS, Demarchi G, Weisz N. Eyes wide shut:
705 Transcranial alternating current stimulation drives alpha rhythm in a state dependent
706 manner. Sci Rep 2016;6:27138. https://doi.org/10.1038/srep27138.
707 [52] Neuling T, Rach S, Herrmann CS. Orchestrating neuronal networks: Sustained after-
708 effects of transcranial alternating current stimulation depend upon brain states. Front
709 Hum Neurosci 2013;7:161. https://doi.org/10.3389/fnhum.2013.00161.
710 [53] Alagapan S, Schmidt SL, Lefebvre J, Hadar E, Shin HW, Fröhlich F. Modulation of

711 cortical oscillations by low-frequency direct cortical stimulation is state-dependent.
712 PLOS Biol 2016;14:e1002424. https://doi.org/10.1371/journal.pbio.1002424.
713 [54] Vieira PG, Krause MR, Pack CC. tACS entrains neural activity while somatosensory
714 input is blocked. BioRxiv 2019:691022. https://doi.org/10.1101/691022.
715 [55] Herring JD, Esterer S, Marshall TR, Jensen O, Bergmann TO. Low-frequency alternating
716 current stimulation rhythmically suppresses gamma-band oscillations and impairs
717 perceptual performance. Neuroimage 2019;184:440–9.
718 https://doi.org/10.1016/j.neuroimage.2018.09.047.
719 [56] Ruhnau P, Keitel C, Lithari C, Weisz N, Neuling T. Flicker-driven responses in visual
720 cortex change during matched-frequency transcranial alternating current stimulation.
721 Front Hum Neurosci 2016;10:184. https://doi.org/10.3389/fnhum.2016.00184.
722

723 **Figures**

724

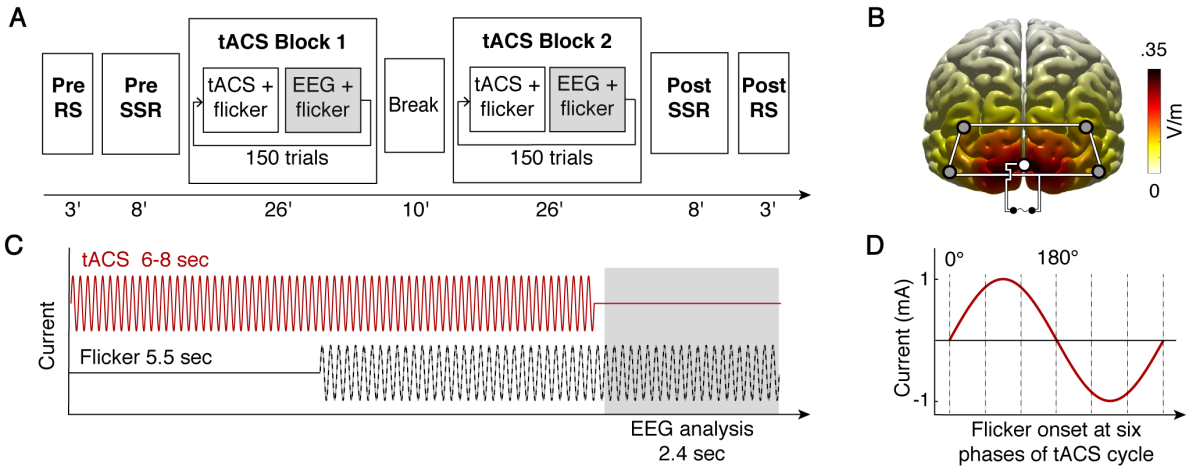

725

726 **Figure 1.** Experimental setup. (A) Schematic display of the experimental timeline. The
727 experiment was conducted on two separate days for active tACS and sham stimulation. Resting
728 state (RS) and visual evoked steady state response (SSR) data without tACS were recorded pre
729 and post to the tACS blocks. (B) tACS electrode montage and power of the tACS-induced
730 stimulation field. The occipital electrode montage induced highest current densities over the
731 primary visual cortex and current spread in surrounding areas. Maximum peak-to-peak
732 difference in field strength is about 0.7 V/m. (C) Illustration of one trial of the intermittent tACS
733 protocol. Each trial started with tACS only, followed by flicker onset after 3-5 sec. The flicker
734 continued for 5.5 sec until the end of the trial. The gray-shaded tACS free intervals were used
735 for EEG data analysis. (D) To vary the phase between neural activity induced by electrical and
736 sensory rhythmic stimulation, visual flicker started at six different phase shifts relative to the
737 tACS cycle. 50 trials per phase angle were presented in randomized order.

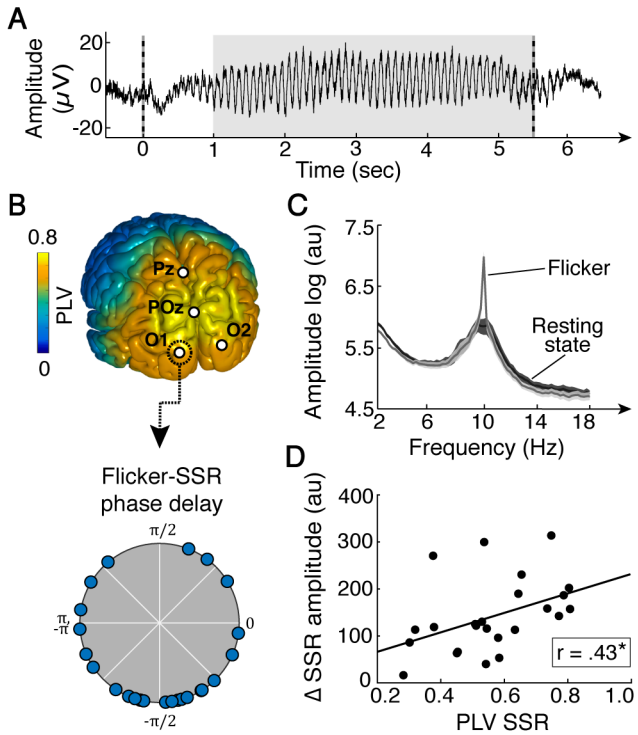

Figure 2. Phase locking values (PLVs) of steady state responses (SSRs) to flicker phase over all trials of the active and sham pre SSR blocks. (A) SSR during 5.5 sec flicker stimulation computed as the average of 50 raw EEG traces of one exemplary participant at channel POz. Dashed lines mark the onset and offset of visual flicker. The gray-shaded area depicts the time window used for EEG data analysis. (B) The upper part depicts the spatial distribution of mean PLVs over all participants with maximal phase locking over the parieto-occipital cortex. Markers correspond to channels selected on sensor level for SSR amplitude analysis. The lower part shows the interindividual variation in phase delays between flicker onset and cortical SSR exemplary for electrode O1. (C) Mean amplitude spectrum during flicker stimulation and resting state over all participants for the four selected channels on sensor level. Shaded areas indicate the standard error. (D) The strength of EEG-flicker PLV at the four parieto-occipital channels is positively correlated with the increase in SSR amplitude from resting state to flicker stimulation during pre SSR blocks across participants ($r = .43$, $p = .037$, n = 24). * $p < .05$.

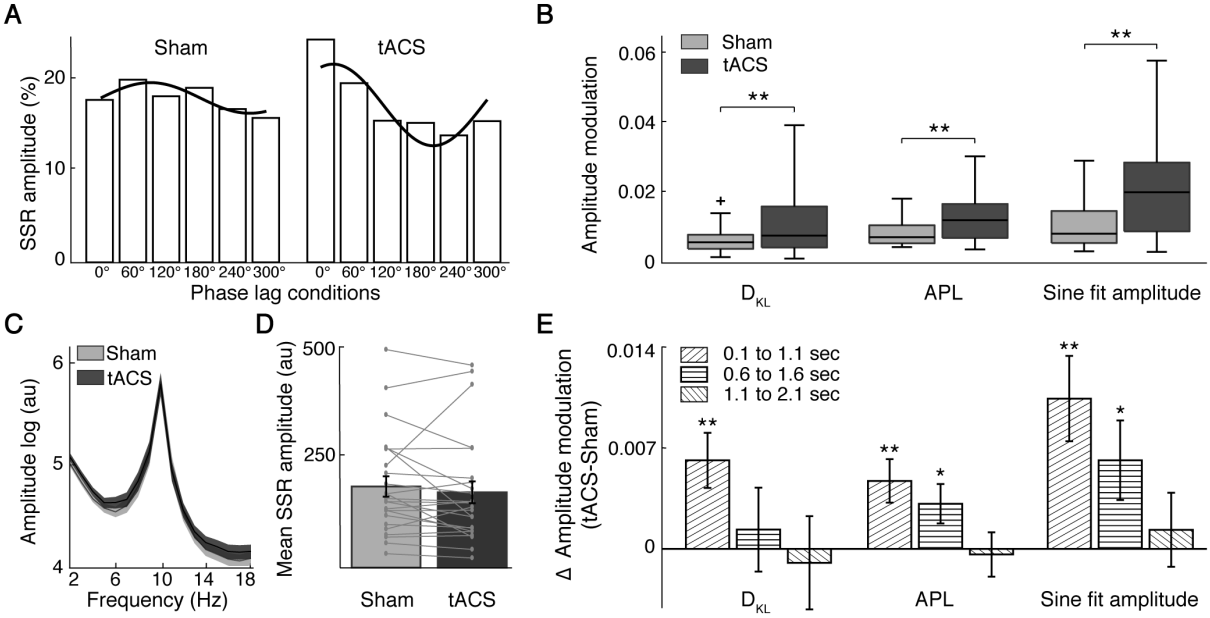

Figure 3. Steady state response (SSR) amplitude modulation by tACS shown for the time window of 0.1 to 1.1 sec after stimulation offset during the tACS block on sensor level. (A) SSR amplitude bar graphs for one exemplary participant. SSR amplitude values differ in the degree of phase dependence under tACS compared to sham. Black lines show sinusoidal fits to the data. (B) Significantly increased Kullback-Leibler divergence (D_{KL}), enhanced phase locking of amplitude values to phase condition (APL) and sine fit amplitudes under tACS relative to sham. (C, D) Phase-dependent amplitude modulation is not paralleled by differences in mean absolute 10 Hz alpha amplitude or mean SSR amplitude over all trials and participants between stimulation conditions. Shaded areas and error bars indicate the standard error. (E) Decay in tACS effect size over three time windows after tACS offset. Bar graphs show the mean difference in SSR amplitude modulation between active and sham tACS condition quantified via three modulation measures. Asterisks mark the uncorrected *p*-value of dependent samples t-tests. Only statistical tests for the first 1 sec time epoch after tACS offset remain significant after Bonferroni correction for comparisons in multiple time windows (α_{bonf} = 0.0167; 0.05/3). Error bars represent the standard error. * $p < .05$; ** $p < .01$.

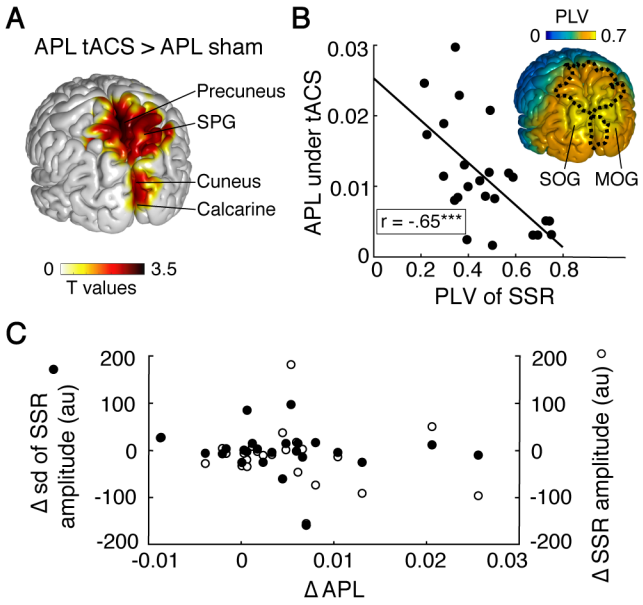

Figure 4. Analysis of tACS-induced amplitude phase locking (APL) of steady state responses (SSRs) during the first 1 sec epoch after tACS. (A) Significant differences in APL between active and sham tACS were localized in a cluster over the parieto-occipital cortex within flicker-entrained brain regions. (B) On sensor level, between-subject correlation shows that the tACS effect size quantified via APL is negatively related to EEG-flicker phase locking (PLV) during the tACS block (r = -.65, p < .001, n = 24). The insert illustrates that after source reconstruction, tACS effects (APL cluster boundary shown as dotted line) are mainly observed in regions where EEG-flicker PLVs did not peak during the tACS block. (C) The increase in APL values under tACS compared to sham is independent of overall changes in mean SSR amplitude or standard deviation (sd) of amplitude values over all trials per participant (sensor level data). MOG, middle occipital gyrus; SOG, superior occipital gyrus; SPG, superior parietal gyrus; *** p < .001.

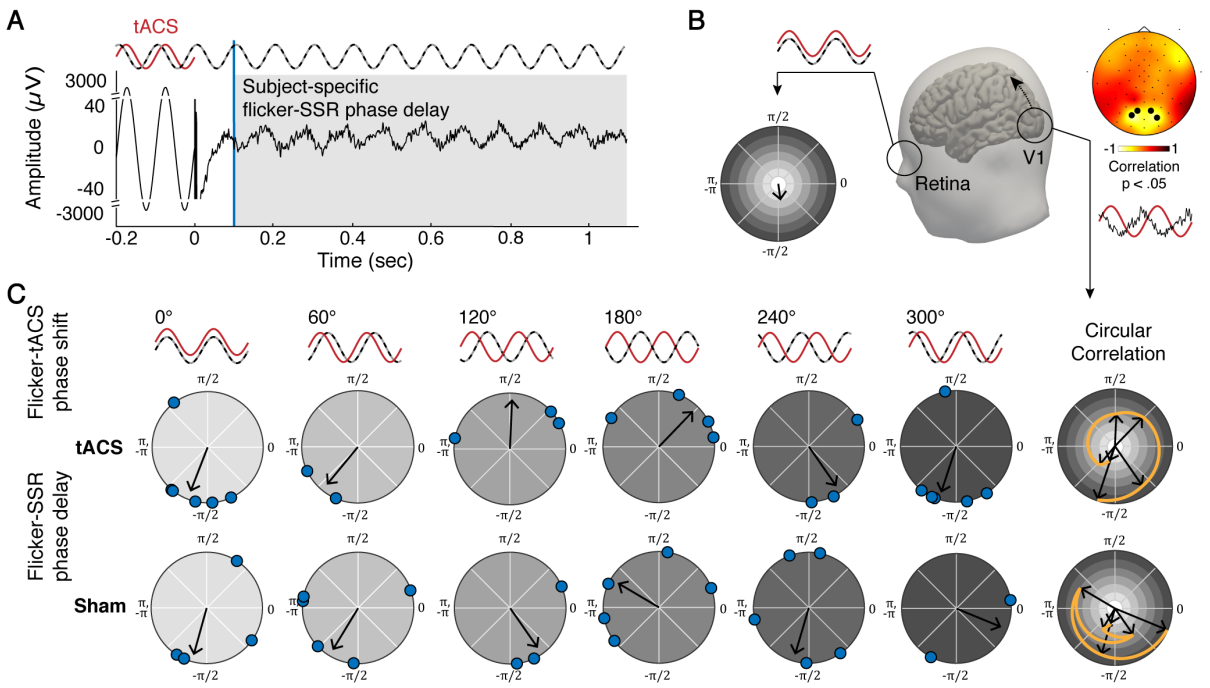

Figure 5. Analysis of the relation between individual cortical SSR onset delays and the optimal timing of tACS application associated with strongest SSRs. (A) Raw EEG data during the tACS block of one representative participant at electrode O1. Data during the last 0.2 sec of tACS stimulation show strong electrical artifacts. The gray-shaded area depicts the time window used for data analysis. (B) In case of an interference of flicker and electric field in the retina, visual response would be modulated before neural conduction delays along the visual pathway take effect. Thus, the optimal flicker-tACS phase shift should be independent of individual SSR onset delays and be comparable across participants as exemplified in the polar plot. In contrast, a significant cluster of occipital electrodes reveals a circular correlation between flicker-tACS phase shift and subject-specific SSR onset delays only during the tACS session. This suggests an interaction of tACS effects and SSR at early stages of visual cortical processing with concurrent spread of activity to higher visual areas. (C) Polar plots show flicker-SSR phase delays for all participants grouped by optimal flicker-tACS phase shift conditions exemplary for electrode O1. Blue circles show the mean flicker-SSR phase delay computed over all trials per participant and arrows depict the mean phase angle over all trials per optimal flicker-tACS

phase shift condition. Circular plots on the right summarize the course of the mean flicker-SSR phase angles over the six flicker-tACS phase shift conditions (gray color code corresponds to flicker-tACS phase shifts of preceding polar plots). During tACS, data show a significant circular correlation between individual SSR phase delays and optimal flicker-tACS phase shifts across participants. There is no significant circular correlation during the sham session.